

On the decay and drift of free-surface perturbations in viscous thin-film flow exterior to a rotating cylinder

E. J. Hinch and M. A. Kelmanson

Proc. R. Soc. Lond. A 2003 **459**, 1193-1213

doi: 10.1098/rspa.2002.1069

Email alerting service

Receive free email alerts when new articles cite this article - sign up in the box at the top right-hand corner of the article or click [here](#)

To subscribe to *Proc. R. Soc. Lond. A* go to: <http://rspa.royalsocietypublishing.org/subscriptions>

On the decay and drift of free-surface perturbations in viscous thin-film flow exterior to a rotating cylinder

BY E. J. HINCH¹ AND M. A. KELMANSON²

¹*Department of Applied Mathematics and Theoretical Physics,
University of Cambridge, Silver Street,
Cambridge CB3 9EW, UK*

²*Department of Applied Mathematics, University of Leeds,
Leeds LS2 9JT, UK (mark@maths.leeds.ac.uk)*

Received 24 January 2002; accepted 11 September 2002; published online 7 March 2003

Free-surface viscous flow exterior to a circular cylinder rotating about its horizontal axis in a vertical gravitational field is considered. When the mean film thickness \bar{h} is small compared with the cylinder radius a , numerical simulations of the full Stokes equations reveal a surface-amplitude decay rate so slow that computational expense precludes investigation of large-time dynamics. However, numerical integrations of the simpler lubrication approximation are achievable to large times, and these reveal not only a slow decay to steady state, but also a gravity-induced phase lag, relative to the cylinder, in the wave modes in the free-surface elevation.

A naive-expansion analysis reveals a complicated evolution in time with four different time-scales. Firstly, there is the fast process of rotating with the cylinder on a time-scale $1/\omega$, where ω is the angular velocity of the cylinder. Secondly, surface tension squeezes the free surface to a cylindrical shape on the time-scale $\mu a^4/\sigma \bar{h}^3$, where μ is the dynamic viscosity of the fluid and σ its surface tension. After this time, disturbances to the steady state take the form of an eccentricity of the cylindrical shape of the free surface that drifts in phase on the third time-scale of $\omega \mu^2 a^2/\rho^2 g^2 \bar{h}^4$, where ρ is the density of the fluid and g the gravitational acceleration, and decays exponentially on the fourth and slowest time-scale of $\omega^2 \mu^3 a^6/\rho^2 g^2 \sigma \bar{h}^7$.

The naive-expansion analysis thus suggests the drift rate and exponential decay rate in the fundamental mode to be proportional to \bar{h}^4 and \bar{h}^7 respectively. A rescaling is suggested wherein \bar{h} is the length-scale, whence a four-term, two-time-scale expansion for the film thickness yields explicit formulae for both the decay and drift rates, the former of which can be used in practical experiments to enforce the fastest possible decay to the steady state. An unusual delay in the resolution of secularity in the two-time-scale expansion is explained, as is the ability of the two-time-scale expansion to capture the four-time-scale physics. Results are presented for a selection of (non-dimensionalized) surface tension and gravity parameters, and excellent agreement is demonstrated between our asymptotics and the results of numerical simulations over varying time-scales. The convergence to the independently derived steady state is demonstrated, and a detailed explanation

is presented of the influential physical mechanisms inherent in the multiple-scale expansion.

Keywords: viscous fluid mechanics; free-surface flow; lubrication approximation; asymptotic expansions; computer algebra

1. Introduction

An overview of the substantial history of the ‘supported-load’ problem—the time-dependent evolution of the free surface of a thin film of viscous fluid adhering to the exterior of a rotating horizontal circular cylinder in a vertical gravitational field—is contained within a recent related paper (Peterson *et al.* 2001) and is not repeated here. The objective of the present paper is to consider a hitherto-unresolved fundamental aspect of this long-standing problem (Moffatt 1977; Pukhnachev 1977): to analyse theoretically the surface-tension-induced decay and gravity-induced drift, relative to the rotating cylinder, of the wave modes in the free surface, and to interpret this analysis in order to identify the controlling physical mechanisms.

Both the drift and decay to steady state are manifest in numerical simulations. In solving the Stokes equations via a novel adaptive finite-element method, Peterson *et al.* (2001) observed that, as the film thickness increases beyond that at which the lubrication approximation is valid, so does the decay rate. However, as the film thickness decreases sufficiently for lubrication theory to be valid, the decay rate becomes so slow that numerical integrations of the Stokes equations are prohibitively expensive, and the simpler lubrication approximation must be used to compute large-time characteristics of the flow. In the present paper, the lubrication approximation of Pukhnachev (1977) is used as the starting point for the analysis.

In §2, a naive-expansion method is used to solve Pukhnachev’s nonlinear fourth-order partial differential equation for the free-surface elevation. The form of the secularity in the higher-order terms in the naive expansion suggests a rescaling of both the gravity and surface-tension parameters, which, in turn, suggest that the mean free-surface elevation, and not the cylinder radius, should be used as the fundamental length-scale. It is inferred that the fundamental mode in the free-surface amplitude decays and drifts at rates proportional to the seventh and fourth powers, respectively, of the film thickness non-dimensionalized with respect to the cylinder radius. Knowing these rates, a rescaling of the lubrication approximation is proposed that is amenable to a multiple-time-scale analysis.

In §3, a four-term two-time-scale expansion is obtained for the free-surface elevation. To obtain the fourth term in this particular case necessitates determination of a particular integral (of a fourth-order partial differential equation in three independent variables) which is so cumbersome that progress is possible only with the aid of an algebraic manipulator. Even then, the problem is rendered tractable only via a simplification based upon the relative magnitude of terms decaying over disparate time-scales. An explanation is given for the curious delay in the resolution of secularity, which occurs not at the expected second but rather the third order in the small parameter. The expansion reveals that four distinct physical processes occur over differing time-scales, and an explanation is given as to why the two-time-scale expansion captures the four-time-scale physics.

In § 4, the multiple-scale expansion is demonstrated to be in excellent agreement with the results of full numerical simulations for ‘large’ times. But since only a two-time-scale expansion is used, it is further demonstrated how the multiple-time-scale results eventually drift from the numerical results at ‘very large’ times; by contrast, the decay rate does not, and this is explained.

In § 5, the steady-state solution is obtained by integrating the governing lubrication approximation to any required degree of accuracy, rather than by considering the infinite-time limit of the solutions gleaned in the previous sections. This is done since the complexity of the time-dependent solutions increases rapidly, and the steady-state solution is more readily obtained via this alternative, more direct, approach. The convergence of the multiple-scale solution to the independently obtained steady state as $t \rightarrow \infty$ is demonstrated.

The paper concludes in § 6 with a physical discussion and interpretation of the preceding mathematics, and the detailed mechanisms occurring on the four time-scales discovered in § 3 are presented. In increasing order of magnitude, these correspond to: rotation with the cylinder; action of surface tension on first and higher harmonics in the free-surface elevation; gravity-induced drift of the fundamental mode; and surface-tension-induced decay of the fundamental mode. Over these time-scales, a complicated and subtle interplay between the compound effects of rotation, gravity and surface tension is revealed. In particular, it is explained how surface tension acts on the slowest time-scale to decay the fundamental wave mode which, being a displaced cylinder, at first sight appears not to admit such action. In this context, a new mechanism, involving the double action of gravity on surface-tension-induced first harmonics, is discovered.

2. Time-scales in the lubrication approximation

In keeping with previous studies, flow variations in the axial direction are neglected. Plane polar coordinates r and θ , centred on the cylinder axis, are employed. Incompressible viscous fluid of thickness $h(\theta, t)$, density ρ and dynamic viscosity μ flows on the exterior of an infinite circular cylinder of radius a rotating anticlockwise about its horizontal axis with angular velocity ω in a gravitational field $\mathbf{g} = -g\hat{\mathbf{j}}$, where $\hat{\mathbf{j}}$ is a unit vector aligned with the positive y -axis and g is the acceleration due to gravity. Surface tension, pressure and flux are denoted by σ , p and q , respectively, and $x = a\theta$ is the arc length around the cylinder surface.

We address the lubrication approximation (rather than the full Stokes equations), for which the dimensional equations for mass conservation, flux and pressure are

$$\partial_t h + \partial_x q = 0, \quad (2.1)$$

$$q = a\omega h - \frac{h^3}{3\mu} \left\{ \rho g \cos\left(\frac{x}{a}\right) - \partial_x p \right\}, \quad (2.2)$$

$$p = \sigma \left\{ \partial_x^2 h + \frac{h}{a^2} \right\}. \quad (2.3)$$

The initial dimensional profile of the free surface is $h(\theta, 0) = h_0(\theta)$.

If length, time, velocity and flux are respectively scaled with respect to a , $1/\omega$, $a\omega$ and $a^2\omega$ as per Pukhnachev (1977), elimination of both q and p from (2.1)–(2.3)

yields the dimensionless thin-film advection–diffusion equation for the 2π -periodic function $h(\theta, t)$ as

$$\partial_t h + \partial_\theta h - \frac{1}{3} \partial_\theta \{ \gamma_0 h^3 \cos \theta - \alpha_0 h^3 \partial_\theta (\partial_\theta^2 h + h) \} = 0, \quad (2.4)$$

which must be solved subject to the initial condition $h(\theta, 0) = h_0(\theta)/a$. Under this scaling, $0 < h_0(\theta)/a \ll 1$, and the dimensionless gravity and surface-tension parameters are respectively

$$\gamma_0 = \frac{\rho g a}{\omega \mu} \quad \text{and} \quad \alpha_0 = \frac{\sigma}{a \mu \omega}. \quad (2.5)$$

In the experimental set-up described by Moffatt (1977), $\alpha_0 \equiv O(1)$. Moreover, for radii a of the cylinder greater than the capillary length $\sqrt{\sigma/\rho g}$ †, we would have

$$\alpha_0 < \gamma_0. \quad (2.6)$$

For a steady state to exist, the condition

$$\gamma_0 (h_{\max}/a)^2 < 1 \quad (2.7)$$

must be satisfied, where one can fix the numerical factor relating h_{\max} , the dimensional maximum film thickness, to \bar{h} , the dimensional mean film thickness, given by

$$\bar{h} = \frac{1}{2\pi} \int_{\theta=0}^{2\pi} h_0(\theta) \, d\theta. \quad (2.8)$$

Then the natural naive expansion $h^{(n)}$ for substitution into (2.4) is

$$h_N^{(n)}(\theta, t) = \sum_{m=1}^N \left(\frac{\bar{h}}{a} \right)^m \phi_m(\theta, t), \quad (2.9)$$

in which the ϕ_m are to be determined.‡

For simplicity, $h_0(\theta)$ is assumed to be constant, h_0 , so that $\bar{h} = h_0$ in (2.9). In the present work, all analytical results were obtained and/or verified using the MAPLE (version 5, release 4) algebraic manipulator (Heck 1996). Indeed, using MAPLE, the determination of ϕ_1 to ϕ_N has been fully automated for arbitrarily large N : this is one advantage of this particular scaling. It transpires that ϕ_m rapidly becomes unwieldy with increasing m , e.g. ϕ_7 contains nine linearly independent harmonics. Despite the relative simplicity of (2.9), it allows some useful conclusions to be drawn at an early stage.

Let $c_{ij} = \cos(i\theta - jt)$, $s_{ij} = \sin(i\theta - jt)$ and $\epsilon = \bar{h}/a$. Secularity caused by the fundamental modes c_{11} and s_{11} resonating with the $(\partial_t + \partial_\theta)h$ term in (2.4) first appears as late as ϕ_7 ; specifically, as $\gamma_0^3 t s_{11}$. Surface tension first appears in ϕ_8 as $\alpha_0 \gamma_0^2 t c_{22}$. Key extractions from higher-order terms of $h_{17}^{(n)}$ are summarized in table 1,

† Approximately 2.7 mm for water, with the largest surface tension.

‡ Although terms of order $O(h^2)$ have been neglected in deriving (2.4), the higher powers of \bar{h}/a in $h_N^{(n)}$ do not perturb the decay rates, as evidenced by the agreement between the theory of §4 and the physics of §6. While it is possible, however, that there may be a second-order perturbation to the theoretically obtained drift, the numerical evidence of §4 suggests that there is not.

Table 1. Subsequences extracted from the naive expansion $h_{17}^{(n)}(\theta, t)$

these components...	... contain...	... and signify
$\phi_3 \rightarrow \phi_{10} \rightarrow \phi_{17}$	$\gamma_0 c_{11} \rightarrow \alpha_0 \gamma_0^3 t c_{11} \rightarrow \alpha_0^2 \gamma_0^5 t^2 c_{11}$	decay of c_{11}
$\phi_3 \rightarrow \phi_7 \rightarrow \phi_{11}$	$\gamma_0 c_{11} \rightarrow \gamma_0^3 t s_{11} \rightarrow \gamma_0^5 t^2 c_{11}$	drift of c_{11}
$\phi_5 \rightarrow \phi_8 \rightarrow \phi_{11}$	$\gamma_0^2 c_{22} \rightarrow \alpha_0 \gamma_0^2 t c_{22} \rightarrow \alpha_0^2 \gamma_0^2 t^2 c_{22}$	decay of c_{22}

in which it is noted that t is non-dimensional. The three rows, from top to bottom, reveal that

- (i) the fundamental mode c_{11} decays on a (dimensional) time-scale of order $O(1/\epsilon^7 \alpha_0 \gamma_0^2 \omega)$;
- (ii) the fundamental mode's phase drifts through s_{11} on a time-scale of order $O(1/\epsilon^4 \gamma_0^2 \omega)$; and
- (iii) the first harmonic c_{22} decays on a time-scale of order $O(1/\epsilon^3 \alpha_0 \omega)$.

Thus the slow time-scale for a multiple-scale analysis should be $1/\epsilon^4 \gamma_0^2 \omega$, and a rescaling is therefore implied in which $\epsilon^2 \gamma_0$ and $\epsilon^3 \alpha_0$ are, respectively, the gravity and surface-tension parameters. Accordingly, we define γ and α by

$$\gamma = \frac{1}{3} \epsilon^2 \gamma_0 \quad \text{and} \quad \alpha = \frac{1}{3} \epsilon^3 \alpha_0, \quad (2.10)$$

wherein the threes in the denominator absorb the numerical factor in (2.4). Taken together, equations (2.6) and (2.10) imply

$$\gamma^2 \ll \alpha \ll \gamma \ll 1 \quad (2.11)$$

when realistic values are given to the physical parameters[†] on the right-hand sides in (2.5). Note that, irrespective of the fluid properties, equation (2.11) can always be established by making ϵ sufficiently small. Note also that, for the reasons given in §3, our subsequent analysis is applicable to unphysically large $O(1)$ values of α . Moreover, as we deduce in §3, the hierarchy of scales within a formal *two*-time-scale expansion automatically admits the *four* time-scales over which the distinct physical mechanisms occur in this problem.

The prediction of a large-time-scale decay in the free-surface wave modes is consistent with the observations of Kuiken (1990), who notes the 'striking difference' between the asymptotic properties of free surfaces which are initially either non-oscillatory or oscillatory. He discovered that, under the action of surface tension and curvature gradients alone, the former is flattened out at a much slower pace than the latter.

It is noteworthy that the reflected fundamental mode $\cos(\theta + t)$ first appears in ϕ_7 , i.e. the amplitude of the reflected fundamental mode $c_{1,-1}$ is $O(\bar{h}^4)$ times smaller than that of the fundamental mode c_{11} , which appears in ϕ_3 . Reflected higher harmonics appear in subsequent terms.

[†] In the experimental set-up of figure 5a in Moffatt (1977), we find $\gamma \sim 0.07$ and $\alpha \sim 10^{-4}$, so that $\alpha \ll \gamma \ll 1$. However, $\gamma^2 \gg \alpha$ and the hierarchy (2.11) is violated, as evidenced by the unstable steepening flow, i.e. the film is too thick for our theory to apply. However, the case $\alpha \ll \gamma^2$ is amenable to (a different) analysis and is discussed briefly in §4; in particular, see figure 6 and the footnote on page 1207.

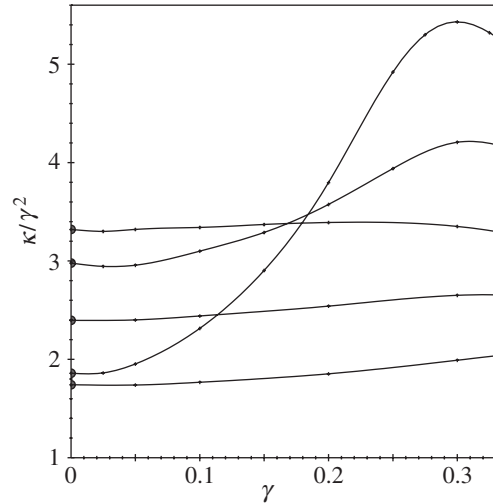


Figure 1. Decay rates, κ , obtained from numerical integration of (2.12). Curves show κ/γ^2 plotted against γ for different α . At the right-hand edge of the plot, curves from top to bottom correspond to $\alpha = 0.025, 0.05, 0.1, 0.2$ and 0.3 . Theoretical values of κ/γ^2 in the limit $\gamma \rightarrow 0$ are given by $\zeta_0(\alpha)$ in (3.13) and are shown by discs on the $\gamma = 0$ axis.

The late appearance of both secularity and surface tension in the naive expansion $h_N^{(n)}(\theta, t)$ strongly suggests a rescaling of (2.4), in which γ_0 and α_0 of (2.5) are replaced by the rescaled parameters γ and α of (2.10). These substitutions made, the more standard lubrication-approximation rescaling of the dimensional h with respect to not a but \bar{h} means that the lubrication approximation (2.4) becomes

$$\partial_t h + \partial_\theta h - \partial_\theta \{ \gamma h^3 \cos \theta - \alpha h^3 \partial_\theta (\partial_\theta^2 h + h) \} = 0, \quad (2.12)$$

which must now be solved subject to the initial condition $h(\theta, 0) = h_0(\theta)/\bar{h}$, which is unity for the given choice of $h_0(\theta)$. Under this scaling, only two non-dimensional parameters, γ and α , are required, whereas three, γ_0 , α_0 and \bar{h}/a (i.e. h_0/a), were required in (2.4) and its associated initial condition. Moreover, the steady-state condition (2.7) becomes $\gamma < \frac{1}{3}$, and, in keeping with (2.11) and the observations of Hansen & Kelmanson (1994), physically realistic values of α are of order $O(h_0^3/a^3) \ll 1$. From the above discussion of the naive expansion, the (non-dimensional) decay and drift time-scales in the fundamental mode are, respectively, predicted to be $1/\alpha\gamma^2$ and $1/\gamma^2$, rates which are indeed confirmed by the numerical experiments summarized in figure 1.

The decay rate κ was calculated from successive maximum amplitudes (at a fixed station θ) obtained via large-time finite-difference integrations of (2.12). Values of κ were obtained for varying α - γ combinations. In figure 1, the ratio κ/γ^2 is plotted against γ for five different values of α . For the higher values of α , it is evident that κ/γ^2 is only weakly dependent on γ . However, the dependence of κ/γ^2 on γ becomes more pronounced as α decreases. A partial explanation of this behaviour can be given following an analysis of the decay rate. Accordingly, discussion is deferred until an explicit form of the decay rate is obtained in § 3. It is noted that, in the limit $\gamma \rightarrow 0$,

the theoretical decay rates given by (3.13), shown in figure 1 by the black discs on the $\gamma = 0$ axis, agree well with those obtained from the numerical experiments.†

3. Multiple-scale analysis

For the analysis in this section, the hierarchy (2.11) of small parameters is assumed, whereupon the $(N + 1)$ -term, two-time-scale expansion

$$h_{N+1}^{(2t)}(\theta, t) = 1 + \sum_{m=1}^N \gamma^m \psi_m(\theta, t_0, t_1) \quad (3.1)$$

is proposed, wherein $t_0 = t$ and $t_1 = \gamma^2 t$, so that $\partial_t = \partial_{t_0} + \gamma^2 \partial_{t_1}$. It should be noted that, despite (2.11), the analysis in this section is indeed applicable when α is as large as $O(1)$. This is because the free-surface elevation is only weakly dependent on α , an observation quantified by Hansen & Kelmanson (1994), whose results indicate this weak dependence over the parameter range $1 \leq \alpha_0 \leq 100$.

It is convenient to define the differential operator

$$\mathcal{L} \equiv \alpha(\partial_\theta^4 + \partial_\theta^2) + \partial_\theta + \partial_{t_0},$$

so that the solution of the homogeneous equation $\mathcal{L}\Psi(\theta, t_0, t_1) = 0$ for the 2π -periodic function $\Psi(\theta, t_0, t_1)$ is

$$\Psi(\theta, t_0, t_1) = \sum_{n=1}^{\infty} [A_n(t_1)c_{nn} + B_n(t_1)s_{nn}] \exp\{-\alpha n^2(n^2 - 1)t_0\}, \quad (3.2)$$

where now $c_{ij} = \cos(i\theta - jt_0)$ and $s_{ij} = \sin(i\theta - jt_0)$, and A_n and B_n are arbitrary functions of t_1 . Equation (3.2) reveals that the n th harmonics $c_{n+1, n+1}$ and $s_{n+1, n+1}$ ($n > 0$) decay exponentially on the time-scale αt_0 . However, the fundamental modes c_{11} and s_{11} can decay only via the functions $A_1(t_1)$ and $B_1(t_1)$ on the slower time-scale $\gamma^2 t_0$, an observation that greatly simplifies matters below.

Substituting expansion (3.1) into (2.12), the order- $O(\gamma)$ problem is

$$\mathcal{L}\psi_1(\theta, t_0, t_1) = -s_{10},$$

with solution

$$\psi_1(\theta, t_0, t_1) = c_{10} + A_1(t_1)c_{11} + B_1(t_1)s_{11}, \quad (3.3)$$

in which the initial condition $h_N^{(2t)}(\theta, 0) = 1$ requires $A_1(0) = -1$ and $B_1(0) = 0$.

At this order, the physical solution $r = a + \bar{h}h \sim a + h_0(1 + \gamma\psi_1)$ gives the free surface as a cylinder whose dimensional radius is $a + h_0$ and whose centre is offset from the axis of the rotating cylinder by the dimensional Cartesian displacement

$$\gamma h_0(1 + A_1 \cos t - B_1 \sin t, -A_1 \sin t + B_1 \cos t). \quad (3.4)$$

This disturbance to the steady state remains cylindrical and rotates with the cylinder on the dimensional time-scale $1/\omega$ (i.e. a non-dimensional time-scale of 1); only on

† Better than this, the subsequent asymptotic analysis applies beyond the small- γ , near-uniform region, as can be seen from the weakly varying curves in figure 1.

a much larger time-scale does the disturbance deviate from a cylindrical profile, via the mechanisms described in § 6.

The order- $O(\gamma^2)$ problem is

$$\mathcal{L}\psi_2(\theta, t_0, t_1) = -3s_{20} - 3A_1(t_1)s_{21} + 3B_1(t_1)c_{21},$$

with solution

$$\begin{aligned} \psi_2(\theta, t_0, t_1) = & \frac{3c_{20}}{2(36\alpha^2 + 1)} - \frac{9\alpha s_{20}}{36\alpha^2 + 1} + \frac{3[A_1(t_1) + 12\alpha B_1(t_1)]c_{21}}{144\alpha^2 + 1} \\ & - \frac{3[12\alpha A_1(t_1) - B_1(t_1)]s_{21}}{144\alpha^2 + 1} + [A_2(t_1)c_{22} + B_2(t_1)s_{22}] \exp\{-12\alpha t_0\}. \end{aligned} \quad (3.5)$$

Thus the first harmonics c_{22} and s_{22} decay naturally on the non-dimensional time-scale $1/\alpha$, so that any term containing them is exponentially small before any variation occurs on either of the much slower non-dimensional time-scales related to drift, $1/\gamma^2$, and decay, $1/\alpha\gamma^2$, predicted immediately after equation (2.10). That these are indeed slower is evident from (2.11), which implies

$$1 \ll \alpha^{-1} \ll \gamma^{-2} \ll \alpha^{-1}\gamma^{-2}.$$

Thus, in the event that α is as (unphysically) large as $O(1)$, this merely states that surface tension acts so rapidly that

$$1 \sim \alpha^{-1} \ll \gamma^{-2} \sim \alpha^{-1}\gamma^{-2},$$

i.e. harmonic decay occurs on the rotation time-scale and fundamental-mode decay occurs on the fundamental-mode drift time-scale. In our non-dimensionalization, the dimensional time-scale for first-harmonic decay is therefore $\mu a^4/\sigma h_0^3$. In fact, equation (3.2) reveals that the n th harmonics, for any $n \geq 1$, decays on this time-scale. Thus, in (3.5), A_2 and B_2 can be considered to be constants that are chosen to satisfy the initial condition $\psi_2(\theta, 0, 0) = 0$. Accordingly, from (3.5), A_2 and B_2 are given by

$$\left. \begin{aligned} A_2 &= -\frac{3}{2(36\alpha^2 + 1)} + \frac{3}{144\alpha^2 + 1}, \\ B_2 &= \frac{9\alpha}{36\alpha^2 + 1} - \frac{36\alpha}{144\alpha^2 + 1}, \end{aligned} \right\} \quad (3.6)$$

wherein $A_1(0) = -1$ and $B_1(0) = 0$ have been used. Note that $A_1(t_1)$ and $B_1(t_1)$ introduced at order $O(\gamma)$ are not determined at order $O(\gamma^2)$.

The order- $O(\gamma^3)$ equation,

$$\mathcal{L}\psi_3(\theta, t_0, t_1) = r_3(\theta, t_0, t_1), \quad \text{say,} \quad (3.7)$$

is cumbersome. In its natural (expanded) form in MAPLE, $r_3(\theta, t_0, t_1)$ contains 145 terms; this figure can be reduced somewhat by judicious manipulation. For example, ten such terms admit the simplification

$$\frac{\{\frac{3}{2}(72\alpha^2 - 1)(36\alpha^2 + 1)[A_1(t_1)^2 + B_1(t_1)^2] - \frac{9}{2} - 648\alpha^2\}s_{10}}{4(144\alpha^2 + 1)(36\alpha^2 + 1)}.$$

A particular solution for (3.7) cannot be obtained until the slow-time functions $A_1(t_1)$ and $B_1(t_1)$ arising at order $O(\gamma)$ are determined. These are found by annihilating the coefficients in $r_3(\theta, t_0, t_1)$ of the resonant fundamental modes c_{11} and s_{11} , where, in keeping with the determination of A_2 and B_2 , terms in $\exp\{-12\alpha t_0\}$ have been dropped. One obtains the coupled secularity equations

$$\partial_{t_1} A_1(t_1) = a_1 A_1(t_1) + b_1 B_1(t_1), \quad (3.8)$$

$$\partial_{t_1} B_1(t_1) = a_2 A_1(t_1) + b_2 B_1(t_1), \quad (3.9)$$

wherein

$$a_1 = b_2 = -\frac{81\alpha}{144\alpha^2 + 1}, \quad (3.10)$$

$$b_1 = -a_2 = \frac{3(72\alpha^2 + 5)}{2(144\alpha^2 + 1)}. \quad (3.11)$$

Equations (3.8) and (3.9) are solved (with t_0 fixed) subject to the initial conditions $A_1(0) = -1$ and $B_1(0) = 0$, to yield

$$A_1(t_1) = -\exp(a_1 t_1) \cos(b_1 t_1) \quad \text{and} \quad B_1(t_1) = \exp(a_1 t_1) \sin(b_1 t_1). \quad (3.12)$$

As $\gamma \rightarrow 0$, the decay rate κ of h will be dominated by that of the order- $O(\gamma)$ term, i.e. $|a_1|\gamma^2$ on the fast time-scale. Therefore,

$$\lim_{\gamma \rightarrow 0} \frac{\kappa}{\gamma^2} = \frac{81\alpha}{144\alpha^2 + 1} = \zeta_0(\alpha), \quad \text{say.} \quad (3.13)$$

The values $\zeta_0(0.025)$, $\zeta_0(0.05)$, $\zeta_0(0.1)$, $\zeta_0(0.2)$ and $\zeta_0(0.3)$ are superimposed on the corresponding α curves in figure 1; the numerics and the theory visibly agree. By inspection of figure 1, κ/γ^2 has a complicated dependence on γ and α . However, the weak dependence of κ/γ^2 on γ for the higher values of α corroborates the physical expectation that increasing the surface tension decays the higher Fourier modes more rapidly, so that the overall decay rate is dictated by that of only the fundamental mode c_{11} .

It is noteworthy that $\zeta_0(\alpha)$, positive for all $\alpha > 0$, has a unique maximum when $\alpha = \frac{1}{12}$; thus the decay rate is maximized when, via (2.5) and (2.10),

$$\bar{h} = \left(\frac{\omega a^4 \mu}{4\sigma} \right)^{1/3}, \quad (3.14)$$

giving the dimensional initial film thickness yielding the fastest decay rate of oscillations in the free surface when the physical parameters of the cylinder and fluid are specified *a priori*. This observation may be useful from a practical point of view.

The resolution of secularity at order $O(\gamma^3)$ may now be explained. Surface tension squeezes the free surface to a cylindrical shape, represented by the fundamental-mode component ψ_1 in (3.3); this squeezing occurs on the non-dimensional time-scale $1/\alpha$. This cylindrical shape, however, rotates with the cylinder and is not steady, changing via the actions of A_1 and B_1 on the much larger time-scale $1/\alpha\gamma^2$ (see (3.10) to (3.12)). Over this time-scale, equation (3.4) implies that the centre of the cylindrical component of the free surface spirals into the point with dimensional Cartesian coordinates $(\gamma h_0, 0)$ relative to the centre of the rotating cylinder. In order to cause

a secular drift in the fundamental modes c_{11} and s_{11} in ψ_1 , it is necessary for the $\gamma \cos \theta$ of gravity to act twice: once to create the first harmonics c_{21} and s_{21} in ψ_2 and then again to force secular terms in the fundamental modes in the problem (3.7) for ψ_3 .

It is this double action of gravity that makes the slow time $t_1 = \gamma^2 t_0$. Gravity acting alone,† however, gives just a drift in phase with no change in amplitude. For a decay in the amplitude of the fundamental mode, surface tension $O(\alpha)$ must act at the intermediate level with the harmonics. This is why the slow decay rate is $O(\alpha\gamma^2)$. It is fortuitous that the ratio $1/\alpha$, of the fundamental-mode decay time-scale to the fundamental-mode drift time-scale, is identical to that of the n th-harmonic decay time-scale to the non-dimensional rotation time-scale of unity. This is why the two-time-scale expansion (3.1) automatically admits all four time-scales governing the distinct physical mechanisms herein. Even if α is as unphysically large as $O(1)$, the four time-scales simply collapse into the two appearing explicitly in (3.1). A detailed description of this four-time-scale interplay between the actions of rotation, gravity and surface tension is deferred until § 6.

The function $\psi_3(\theta, t_0, t_1)$ can now be found. With the fast-time-scale exponential terms neglected in (3.7), 66 terms disappear from the 145-term expanded form of $r_3(\theta, t_0, t_1)$, and, when the order- $O(\gamma)$ slow-time-scale solutions in (3.12) are imposed, $r_3(\theta, t_0, t_1)$ reduces further to a linear combination of the ten harmonics c_{10} , s_{10} , c_{12} , s_{12} , c_{30} , s_{30} , c_{31} , s_{31} , c_{32} and s_{32} . The A_3 and B_3 terms appearing in the solution at order $O(\gamma^3)$ are, via (3.2), multiplied by $\exp\{-72\alpha t_0\}$. In parallel with the argument used to determine A_2 and B_2 , A_3 and B_3 are chosen simply to satisfy the initial condition $\psi_3(\theta, 0, 0) = 0$. However, at this order, the modes c_{10} , s_{10} , c_{12} and s_{12} violate the initial condition unless the particular integral is supplemented by a suitable linear combination of c_{11} and s_{11} (both of which are annihilated by the operator \mathcal{L} in (3.7)). Hence $\psi_3(\theta, t_0, t_1)$ is determined as a linear combination of 12 harmonics, the coefficients of which are so cumbersome that the explicit expression for $\psi_3(\theta, t_0, t_1)$ is not presented.

Figure 2 illustrates the convergence (towards the results of numerical simulations) of $h_{N+1}^{(2t)}(\theta, t)$ when $N + 1 = 2, 3$ and 4 in (3.1). Results are presented at the station $\theta = 0$ in the time-interval $0 \leq t \leq 10$. From the close agreement between $h_4^{(2t)}(0, t)$ and the numerical results, it is inferred that the neglect of higher-order terms is justified. Moreover, as discussed below, the effect of neglecting such terms is, in any case, dominated by the present restriction to only two time-scales.

4. Amplitude decay and phase drift

From (3.12), the fundamental mode c_{11} decays at the rate $|a_1|\gamma^2$. The corresponding expression for its drift rate through s_{11} is now determined.

In figure 3 are compared results of both the four-term naive and multiple-scale expansions; since $\phi_2 = \phi_4 = \phi_6 = 0$ in (2.9), these are, respectively, $h_7^{(n)}(\theta, t)$ and $h_4^{(2t)}(\theta, t)$. Both expansions are further compared with the benchmark results of an explicit 50-node, fourth-order central-finite-difference method applied to (2.12). Results are presented at the station $\theta = 0$. The comparison is meaningful only for

† Note that $\alpha \equiv 0$ results in wave breaking due to propagation of undamped harmonics of $h_0(\theta)$ at different speeds; for periodic motion, non-zero surface tension, however small, is required.

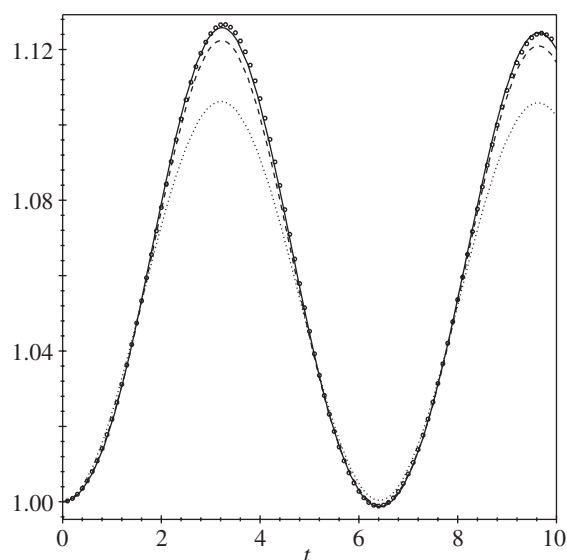


Figure 2. Convergence of two-time-scale expansion to numerical results: two-term, two-time-scale expansion $h_2^{(2t)}(0, t)$ (dotted line), three-term, two-time-scale expansion $h_3^{(2t)}(0, t)$ (dashed line), four-term, two-time-scale expansion $h_4^{(2t)}(0, t)$ (solid line) and 50-node, fourth-order finite-difference results (circles). Here, $\gamma = 0.0532$ and $\alpha = 0.0048$, corresponding to $\gamma_0 = 12.5$, $\alpha_0 = 10$ and $h_0/a = 0.11298$.

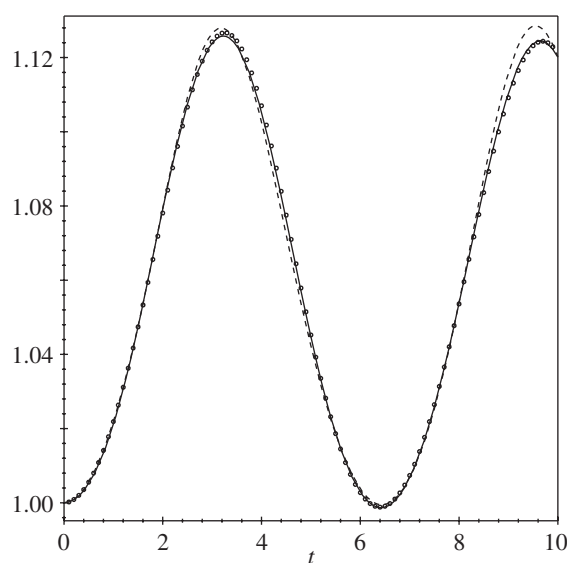


Figure 3. Small-time comparison of four-term naive expansion $h_7^{(n)}(0, t)$ (dashed line), four-term, two-time-scale expansion $h_4^{(2t)}(0, t)$ (solid line) and 50-node, fourth-order finite-difference results (circles). Here, $\gamma = 0.0532$ and $\alpha = 0.0048$, corresponding to $\gamma_0 = 12.5$, $\alpha_0 = 10$ and $h_0/a = 0.11298$. The secularity in $h_7^{(n)}(0, t)$ is already evident.

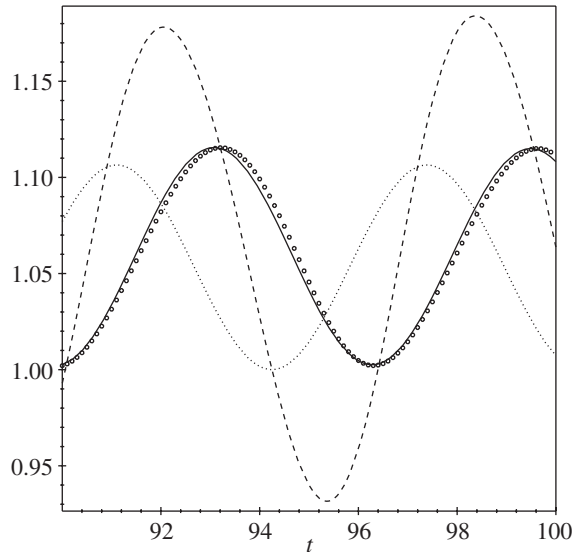


Figure 4. Large-time comparison of four-term naive expansion $h_7^{(n)}(0, t)$ (dashed line), four-term, two-time-scale expansion $h_4^{(2t)}(0, t)$ (solid line) and 50-node, fourth-order finite-difference results (circles). Here, $\gamma = 0.0532$ and $\alpha = 0.0048$, corresponding to $\gamma_0 = 12.5$, $\alpha_0 = 10$ and $h_0/a = 0.11298$. The secularity in $h_7^{(n)}(0, t)$ is now pronounced. Also shown is the two-term naive expansion $h_3^{(n)}(0, t)$ (dotted line), which is stationary relative to the cylinder surface; the separation between the dotted line and the solid line illustrates the phase drift in the free surface.

small times (here, $0 \leq t \leq 10$), before the secular terms in the naive expansion overwhelm the solution. Numerical results for 100 nodes differ imperceptibly, on the presented scale, from those of the 50-node simulation, and the time-step that satisfies the stability criterion ensures that the truncation error of the scheme is of order $O((\Delta\theta)^4)$.

Figure 3 demonstrates the close agreement in $0 \leq t \leq 10$ between $h_4^{(2t)}(0, t)$ and the numerical results; by contrast, the phase of $h_7^{(n)}(0, t)$ drifts ahead of both and its increasing amplitude is already evident.

In figure 4, $h_7^{(n)}(0, t)$ and $h_4^{(2t)}(0, t)$ are again compared with the numerical results, but in the time-interval $90 \leq t \leq 100$. Now, the secularity of the naive expansion is most pronounced, yet the two-time-scale and numerical results remain in close agreement. The non-physical two-term naive expansion $h_3^{(n)}(0, t)$ is non-secular and does not drift relative to the cylinder. Hence the separation between $h_3^{(n)}(0, t)$ and $h_4^{(2t)}(0, t)$, measured in figure 4 to be approximately 2, represents the accumulated drift of the free surface relative to the cylinder. Figure 4 also reveals the first signs of an accumulated drift between $h_4^{(2t)}(0, t)$ and the numerical results, a drift which results from the present restriction to only two time-scales, t_0 and t_1 .

Equations (3.1), (3.3) and (3.12) yield

$$h_2^{(2t)}(\theta, t) = 1 + \gamma \{ \cos \theta - \exp\{a_1 \gamma^2 t\} \cos(\theta - [1 - b_1 \gamma^2]t) \},$$

whence the accumulated lag in the fundamental mode in the free-surface elevation at time t is

$$A(t) = \frac{b_1 \gamma^2 t}{1 - b_1 \gamma^2}. \quad (4.1)$$

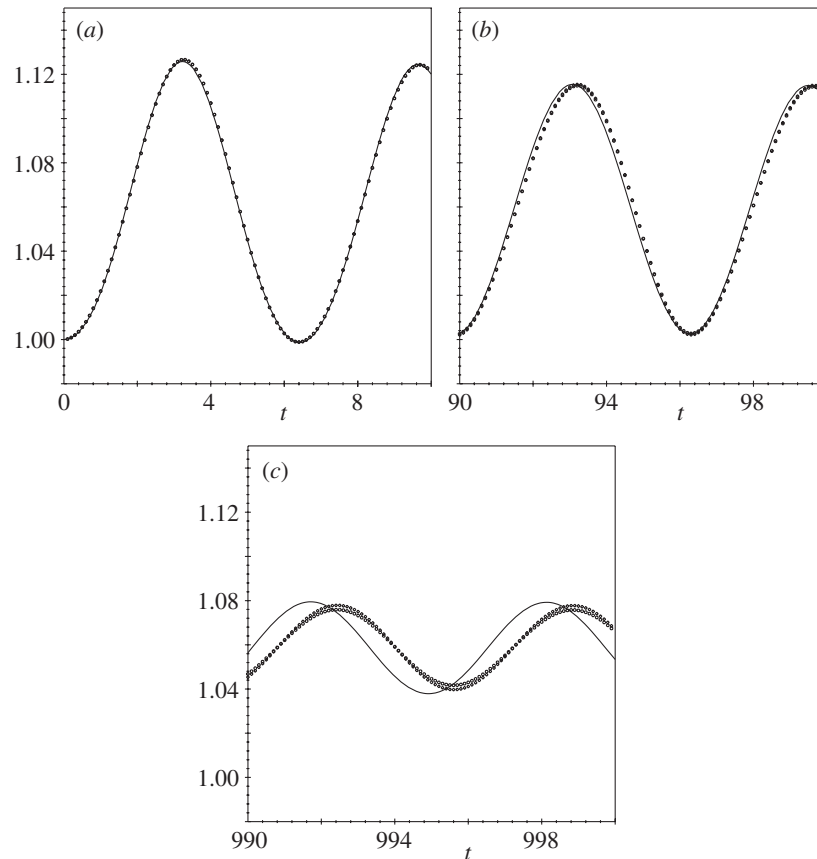


Figure 5. Eventual drift of four-term, two-time-scale expansion $h_4^{(2t)}(0, t)$ (solid line) relative to 50-node, fourth-order finite-difference results (circles) and 100-node, fourth-order finite-difference results (diamonds). (a) $0 \leq t \leq 10$. (b) $90 \leq t \leq 100$. (c) $990 \leq t \leq 1000$. Here, $\gamma = 0.0532$ and $\alpha = 0.0048$, corresponding to $\gamma_0 = 12.5$, $\alpha_0 = 10$ and $h_0/a = 0.11298$.

With $\gamma = 0.0532$ and $t = 95$ (the mid-point of the time-interval in figure 4), $\Lambda(t) \simeq 2.0528$, which compares well with the numerically obtained figure cited above.

At later times, the accuracy of the two-time-scale expansion is expected to deteriorate. This deterioration is demonstrated in figure 5, which shows a comparison of $h_4^{(2t)}(0, t)$ with the results of both 50- and 100-node finite-difference integrations during the three time-intervals $0 \leq t \leq 10$, $90 \leq t \leq 100$ and $990 \leq t \leq 1000$ when $\gamma = 0.0532$ and $\alpha = 0.0048$. In figure 5c, it is evident that the two-time-scale expansion has drifted appreciably from the (mutually confirming) finite-difference results, indicating that the order- $O(\gamma^2)$ perturbation in period requires further correction, almost certainly on the time-scale $t_2 = \gamma^4 t$. However, despite this large-time drift in the phase of the fundamental mode c_{11} , its amplitude remains well represented. This is because the decay and drift time-scales, from (3.10) and (3.11), are here approximately $81\alpha\gamma^2 t \sim 0.001t$ and $\frac{15}{2}\gamma^2 t \sim 0.02t$, respectively. Hence the phase and amplitude will remain well represented by the two-time-scale expansion up to times of 50 and 1000, respectively. Prolongation of these times would require the

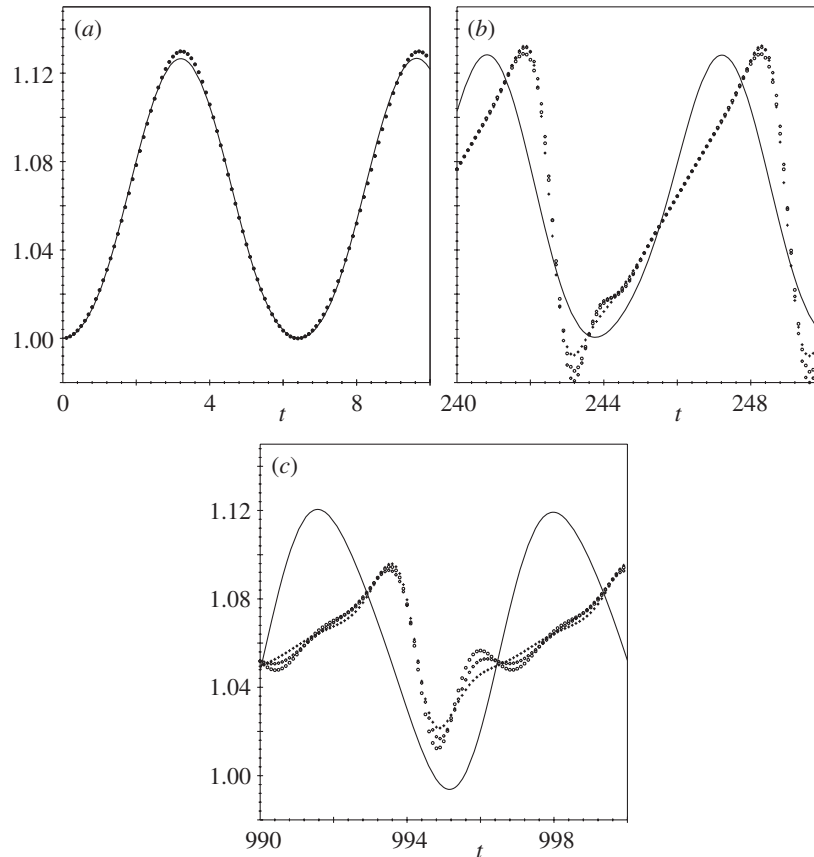


Figure 6. Effect of violation of (2.11) as $\alpha \rightarrow 0$. Four-term, two-time-scale expansion $h_4^{(2t)}(0, t)$ (solid line) compared with finite-difference results with: $\Delta\theta = 2\pi/50$, $\Delta t = (\Delta\theta)^4$ (circles); $\Delta\theta = 2\pi/50$, $\Delta t = \alpha_0(\Delta\theta)^4$ (diamonds); $\Delta\theta = 2\pi/100$, $\Delta t = (\Delta\theta)^4$ (plus signs). (a) $0 \leq t \leq 10$. (b) $240 \leq t \leq 250$. (c) $990 \leq t \leq 1000$. Here, $\gamma = 0.0532$ and $\alpha = 0.000\,048$, corresponding to $\gamma_0 = 12.5$, $\alpha_0 = 0.1$ and $h_0/a = 0.112\,98$.

inclusion of the slower time-scale $t_2 = \gamma^4 t$, which would require the solution of the order- $O(\gamma^4)$ equation for ψ_4 .

The approximate expression (4.1) for drift was obtained on the basis of the physically realistic assertion that $0 < \alpha \ll 1$. Care should be taken when considering the limit $\alpha \rightarrow 0$, since then (2.11) is violated. This is demonstrated in figure 6, which shows results analogous to those in figure 5, but now with α reduced from 4.8×10^{-3} to 4.8×10^{-5} .

Figure 6 confirms the expectation that violation of (2.11) leads to a breakdown in the two-time-scale theory, whose results clearly depart from the mutually confirming numerical results. In particular, figure 6*b* reveals a sharp steepening of the rotating wavefront *counter* to the direction of rotation (slow increase followed by sharp drop), similar to that observed by both Wilson & Williams (1997)—in the related rimming-flow problem—and Peterson *et al.* (2001), wherein parts (d) and (e) of figure 9 portray the onset of dripping. Most interestingly, the numerical results in figure 6*c*

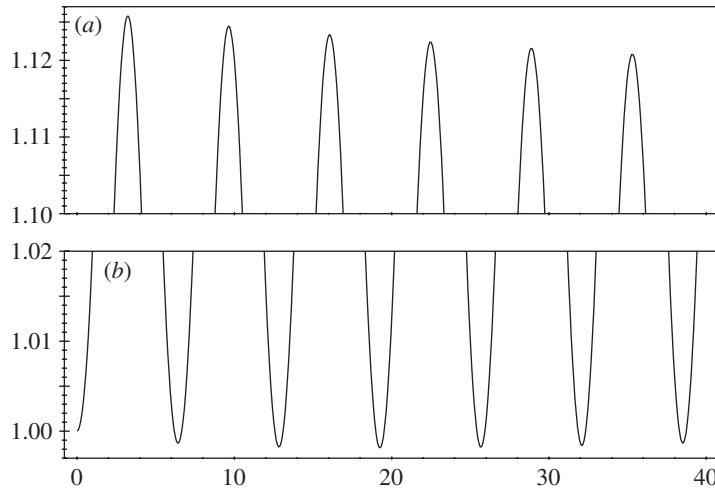


Figure 7. Detail of (a) maxima and (b) minima of $h_4^{(2t)}(0, t)$ during $0 \leq t \leq 40$. Here, $\gamma = 0.0532$ and $\alpha = 0.0048$, corresponding to $\gamma_0 = 12.5$, $\alpha_0 = 10$ and $h_0/a = 0.11298$.

indicate an algebraic (rather than exponential) decay, in keeping with shock-like solutions.†

The two-time-scale expansion $h_4^{(2t)}(\theta, t)$ reveals an unexpected feature of the free-surface elevation at a given station θ . In the presence of non-zero surface tension, it is reasonable to expect that the maximum and minimum elevation, respectively, will be monotone-decreasing and increasing functions of t . This is not the case. For certain α - γ combinations, rather complicated behaviour occurs in which both/either the maximum and/or minimum themselves oscillate with t before eventually becoming monotone towards the steady state.

Figure 7 shows an example of this, in which the maximum does indeed decrease for all $t > 0$, even though the minimum first decreases before eventually increasing. However, the amplitude is a decreasing function of t and, during the period in which the minimum drops, the maximum does so even more rapidly. If α is decreased below the value shown, the time until the reversal of the minimum is increased beyond that shown. This varied and complicated behavioural dependence on the parameters α and γ , combined with the slow natural decay rate, makes the observation of amplitude decay extremely expensive and/or difficult when the full Stokes approximation is studied numerically (Peterson *et al.* 2001).

5. Approach to steady state

Since higher-order terms in the steady-state solution can be found from none of the expansions so far determined, the steady-state expansion, $h_N^{(s)}(\theta)$, is now derived. Setting $\partial_t h = 0$ in (2.12) and integrating once with respect to θ yields

$$h - \gamma h^3 \cos \theta + \alpha h^3 \partial_\theta (\partial_\theta^2 h + h) = h_\infty,$$

† The case $\alpha \ll \gamma^2$ (and other regimes) has been solved while this paper was under submission, and the shock-like solutions have been extensively analysed; these results are the subject of a companion paper.

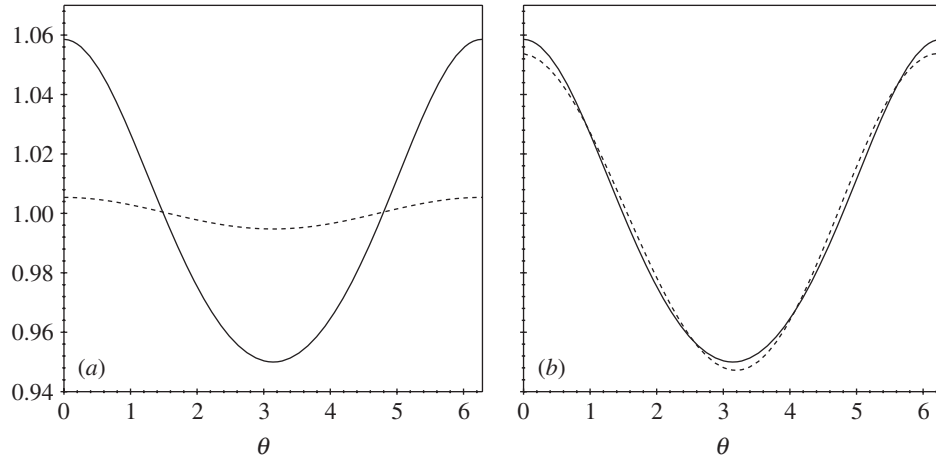


Figure 8. Variation of steady-state free-surface profiles, represented by four-term, steady-state expansion $h_4^{(s)}(\theta)$, with both gravity and surface tension. (a) With $\alpha = 0.0048$: $\gamma = 0.0532$ (solid line); $\gamma = 0.00532$ (dashed line). (b) With $\gamma = 0.0532$: $\alpha = 0.0048$ (solid line); $\alpha = 0.48$ (dashed line), which is unphysically large by a factor of approximately 100.

where h_∞ is an unknown constant. The natural expansions are therefore

$$h_{N+1}^{(s)}(\theta) = 1 + \sum_{m=1}^N \gamma^m \xi_m(\theta) \quad \text{and} \quad h_\infty = 1 + \sum_{m=1}^N \gamma^m \rho_m,$$

wherein the requirement that each $\xi_m(\theta)$ is 2π -periodic dictates the values of ρ_m . The solution procedure is readily automated using MAPLE. The expansion when $N = 4$ is

$$h_4^{(s)}(\theta) = 1 + \gamma c_{10} + \frac{3\gamma^2(c_{20} - 6\alpha s_{20})}{2(36\alpha^2 + 1)} + \frac{3\gamma^3}{2(36\alpha^2 + 1)} \\ \times \left\{ 3(c_{10} - 6\alpha s_{10}) - \frac{2(234\alpha^2 - 1)c_{30} - 6\alpha(144\alpha^2 - 11)s_{30}}{576\alpha^2 + 1} \right\}, \quad (5.1)$$

with which the compatible constant of integration is $h_\infty = 1 - 3\gamma^2/2 + O(\gamma^4)$. Note that $\xi_m(\theta)$ is readily obtained via this approach, but not from the alternative expressions $\lim_{t \rightarrow \infty} \psi_m(\theta, t, \gamma^2 t)$, which remain undetermined for $m \geq 4$.

As can be seen from figure 8, the free-surface steady state is far more sensitive to changes in gravity than in surface tension, in accordance with the conclusions of Hansen & Kelmanson (1994). Note that, in figure 8b, an unphysically large value of α has been used to corroborate the assertion at the start of § 3 that the expansion results were valid for $\alpha = O(1)$. For a comprehensive treatise on the effects of surface tension on the geometry of steady-state profiles in the context of the intimately related (interior) rimming-flow problem, the reader is referred to the recent papers by Tirumkudulu & Acrivos (2001) and Ashmore *et al.* (2003).

Figure 9 demonstrates the manner in which the steady solution $h_4^{(s)}(\theta)$ is approached by $h_4^{(2t)}(\theta, t)$ as $t \rightarrow \infty$. The period of the fundamental mode c_{11} is, via (4.1), $2\pi/(1 - b_1\gamma^2)$, which, for the parameters used in figure 9, is approximately 2.0433π . Although there is much oscillatory activity between the snapshots

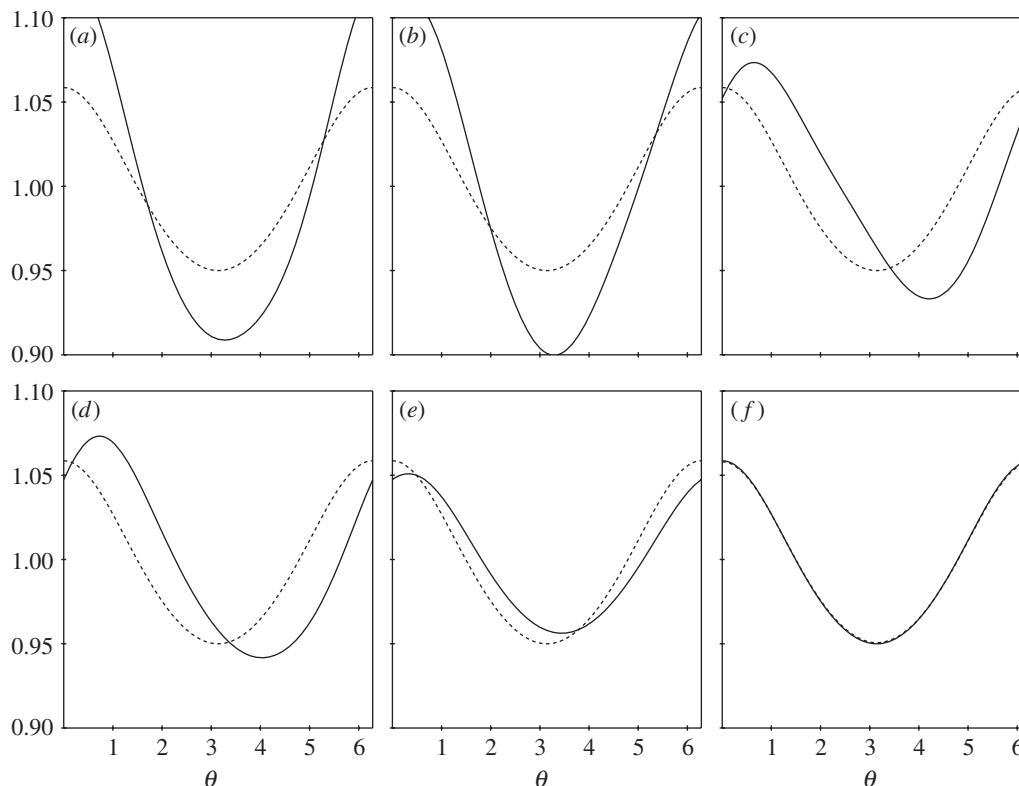


Figure 9. Temporal snapshots of decay to steady state, showing convergence of four-term, two-time-scale expansion $h_4^{(2t)}(\theta, t)$ (solid line) to four-term, steady-state expansion $h_4^{(s)}(\theta)$ (dashed line). (a) $t = 10$. (b) $t = 10^2$. (c) $t = 10^3$. (d) $t = 10^4$. (e) $t = 10^5$. (f) $t = 10^6$. Here, $\gamma = 0.0532$ and $\alpha = 0.000\,048$, corresponding to $\gamma_0 = 12.5$, $\alpha_0 = 0.1$ and $h_0/a = 0.112\,98$.

of parts (a) to (d) of figure 9, MAPLE animations reveal a persistent and barely perceptible undulation, with the period just calculated, between and beyond parts (e) and (f); this is despite the fact that static images at very large times are indistinguishable on the scale presented.

Thus, in practical engineering terms, truly enormous time-scales may be required in order to achieve a steady state. In this light, our theory constitutes a tool for determining the time-scales required to achieve specified tolerances of departure from a uniform state.

Note that, if the fundamental-mode component of the general dimensionless initial profile $h_0(\theta)/\bar{h}$ is identical to the γc_{10} of the steady state in (5.1), convergence to the steady state will be on the fast time-scale $1/\alpha$. However, without loss of generality, this component will differ—as it does for the choice $h_0(\theta) = h_0$ in §§ 2 and 3—and the approach to steady state will be on the largest time-scale $1/\alpha\gamma^2$.

6. Physical mechanisms in the approach to steady state

Finally, an explanation is presented of the mechanisms governing the slow approach to the steady state, i.e. the physics underlying the preceding mathematics is consid-

ered. The explanation is unexpectedly complicated and subtle, revealing a delicate interplay between rotation, gravity and surface tension.

In §§ 2 and 3, the non-dimensional lubrication equation (2.12) is studied for a thin film of viscous fluid rotating on the outside of a horizontal cylinder in a regime where gravity and surface tension satisfy $\alpha \ll \gamma \ll 1$. The leading-order solution is

$$h(\theta, t) \sim h(\theta - t, 0),$$

representing the initial shape $h(\theta, 0)$ simply rotating with the cylinder. Here, the flow is on the fastest time-scale, $1/\omega$ in dimensional terms. Thus, at leading order, the only steady state is a film of uniform thickness, $h \sim 1$, as in (3.1) or (5.1). Further approximations to the steady state are subsequently considered, with corrections coming from small gravity and small surface tension.

In the steady state, the volume flux around the cylinder must be constant, independent of position, so that, on the ‘rising’ side, where gravity slows down the film, the free-surface elevation must be a little thicker than the mean, while on the faster ‘falling’ side, it will be a little thinner. The maximum effect is where gravity is parallel to the film, i.e. on the horizontal level of the axis of the cylinder, with the maximum thickness at $\theta = 0$ and the minimum thickness at $\theta = \pi$. Thus the second approximation to the steady state is

$$h \sim 1 + \gamma \cos \theta, \quad (6.1)$$

again as in (3.1) or (5.1).

The gravity force on the film increases proportionally to the local thickness. This force is equal to the viscous stress at the wall, and so the shear rate in the film increases with its thickness. Hence the change in velocity of the film increases quadratically with thickness, and so the contribution from gravity to the volume flux increases cubically. The contribution from the rotation, however, increases only linearly. Thus, because gravity has such a strong nonlinear effect, the region of the maximum thickness at $\theta = 0$ will be augmented, while the region of the minimum thickness at $\theta = \pi$ will be reduced. Thus the third approximation to the steady state is

$$h \sim 1 + \gamma \cos \theta + \frac{3}{2}\gamma^2 \cos 2\theta,$$

as in (3.5) or (5.1). The coefficient $\frac{3}{2}$ has ‘3’ from the cubic nonlinearity and ‘ $\frac{1}{2}$ ’ from the $\cos 2\theta$ part of $\cos^2 \theta$. The addition of the second harmonic makes the peak near $\theta = 0$ narrower and a little higher, and the trough near $\theta = \pi$ flatter and a little less low.

The effect of a little surface tension is now considered. This acts on only the first- and higher-order harmonics because, at leading order, the fundamental mode is simply a circular cylinder translated along the $\theta = 0$ direction by an amount γ (in h - θ space) (see § 3). There will thus be a capillary pressure, which is positive at $\theta = 0$ and π (the ‘sides’) and negative at $\theta = \frac{1}{2}\pi$ and $\frac{3}{2}\pi$ (the ‘top’ and ‘bottom’, respectively). The capillary pressure gradient therefore speeds up the flow in the first and third quadrants, which thins the film there a little, and slows down the flow in the second and fourth quadrants, wherein the film is correspondingly thickened. Thus the fourth approximation to the steady shape is

$$h \sim 1 + \gamma \cos \theta + \frac{3}{2}\gamma^2 \cos 2\theta - 9\alpha\gamma^2 \sin 2\theta,$$

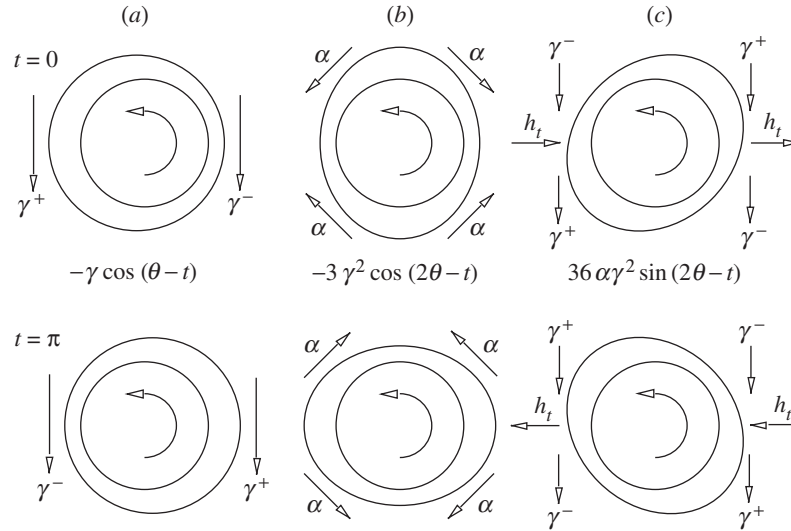


Figure 10. The decay mechanism of the fundamental mode. The two rows are for the disturbance at time $t = 0$ and π , respectively. (a) Gravity acts on the fundamental mode to create the first harmonic in (b). (b) Capillary pressure gradients act to create the phase-shifted first harmonic in (c). (c) Gravity acts on the phase-shifted first harmonic to create a rate of change of amplitude of the fundamental mode.

as in (3.5) and (5.1). This modification due to surface tension makes the shape a little asymmetric with a slow increase in the thickness with θ and a sharp decrease (see figure 6). It also moves both the maximum and minimum film thickness down below the level of the axis, to $\theta = 2\pi^-$ and $\theta = \pi^+$, respectively.

Next, the disturbance to the steady state and the mechanisms by which it decays are considered. The difference between the initial uniform thickness and the eventual steady state represents the initial disturbance

$$\Delta h(\theta, 0) = -\gamma \cos \theta - \frac{3}{2}\gamma^2 \cos 2\theta + 9\alpha\gamma^2 \sin 2\theta + O(\gamma^3).$$

To a first approximation, this disturbance simply rotates without change of form,

$$\Delta h(\theta, t) = \Delta h(\theta - t, 0),$$

on the dimensional time-scale $1/\omega$ (see (3.3) with the initial values $A_1 = -1$ and $B_1 = 0$).

On a longer time-scale, surface tension squeezes the shape circular, i.e. it removes the first harmonic on a non-dimensional time-scale $1/12\alpha$ (see (3.5)), which is a dimensional time of $\mu a^4/\sigma h_0^3$. Surface tension cannot have a direct effect on the fundamental mode, which, as noted above, represents a cylindrical shape of the free surface shifted off centre from the axis of the cylinder through a distance γ . Surface tension does, however, have a complicated *indirect* action on the fundamental mode, resulting in the generation of a new first harmonic through the intermediate action of gravity, and then a second action of gravity on the surface-tension-affected first harmonic to change the original fundamental mode.

At time $t = 0$, the fundamental-mode disturbance, $-\gamma \cos(\theta - t)$, represents a film that is thinner than the steady state near $\theta = 0$ and thicker on the opposite side

near $\theta = \pi$ (see figure 10). Hence the slowing down by gravity at $\theta = 0$ is a little less than in the steady state, while speeding up at $\theta = \pi$ is a little more, as in figure 10*a*. Hence, due to gravity acting on the fundamental-mode disturbance, the film at $t = 0$ is less thickened at $\theta = 0$ and more thinned at $\theta = \pi$; both effects are described by an induced first harmonic $-3\gamma^2 \cos 2\theta$ at $t = 0$. A similar argument at time $t = \pi$ finds a gravitationally induced first harmonic of the opposite sign. This explains the first-harmonic disturbance

$$-3\gamma^2 \cos(2\theta - t) \quad (6.2)$$

in (3.5) with $A_1 = -1$ and $B_1 = 0$.

This gravitationally induced first harmonic, being non-cylindrical, is now acted upon by surface tension. At time $t = 0$, there will be a positive capillary pressure at the top and bottom of the cylinder, and a negative pressure on the sides (see figure 10*b*). Capillary pressure gradients will act to slow, and therefore thicken, the film in the first and third quadrants; similar thinning occurs in the second and fourth quadrants. The signs are reversed at time $t = \pi$, following the reversal of the sign in the gravitationally induced first harmonic (6.2). Hence the surface tension leads to an additional, surface-tension-corrected, first-harmonic disturbance

$$36\alpha\gamma^2 \sin(2\theta - t), \quad (6.3)$$

as in (3.5) with $A_1 = -1$ and $B_1 = 0$.

The gravitationally induced first harmonics (6.2) and (6.3) are very similar to the corresponding terms in the steady state (5.1). The different numerical coefficients are due to the propagation of these first harmonics at a phase speed of $\frac{1}{2}$, corresponding to the fundamental mode propagating at a speed of unity, being viewed through the static fundamental-mode filter of gravity.

Finally, to find how the fundamental-mode disturbance decays slowly in time, the action of gravity on the surface-tension corrections is considered. At time $t = 0$, the fundamental-mode disturbance is $-\gamma \cos \theta$ (see (6.1)), and the surface-tension correction to the gravitationally induced first harmonic is $36\alpha\gamma^2 \sin 2\theta$ (see (6.3)). This first harmonic represents a thickening in the first and third quadrants and a thinning in the second and fourth. Gravity slows down the film in the first and fourth quadrants and speeds it up in the second and third (see figure 10*c*). Combining these two spatial variations yields a slowing down, enhanced in the first quadrant and reduced in the fourth, which produces a net convergence onto $\theta = 0$. Similarly the speeding up is reduced in the second quadrant and enhanced in the third, which produces a net divergence from $\theta = \pi$. Thus the thickness of the film should increase in the region near $\theta = 0$ and decrease on the opposite side near $\theta = \pi$. Thus the amplitude of the fundamental-mode disturbance $-\gamma \cos \theta$ decreases, at a rate calculated to be $54\alpha\gamma^3 \cos \theta$, giving a decay rate of $54\alpha\gamma^2$. The above argument was for the phases of the propagating disturbance at time $t = 0$; the argument for time $t = \pi$ is the same.

There is a second mechanism that contributes further to the decay of the fundamental-mode disturbance (6.1) (see figure 11). The gravitationally induced first harmonic (6.2) calculated above, $-3\gamma^2 \cos(2\theta - t)$, has, at time $t = 0$, a capillary pressure gradient $O(\alpha\gamma^2)$ away from the top and bottom towards the sides at $\theta = 0$ and π . This pressure gradient acting on the fundamental-mode variation of thickness in the steady shape, $\gamma \cos \theta$, produces an increased flux towards $\theta = 0$ and a reduced flux towards $\theta = \pi$. Thus the film is thickened near $\theta = 0$ and thinned near $\theta = \pi$,

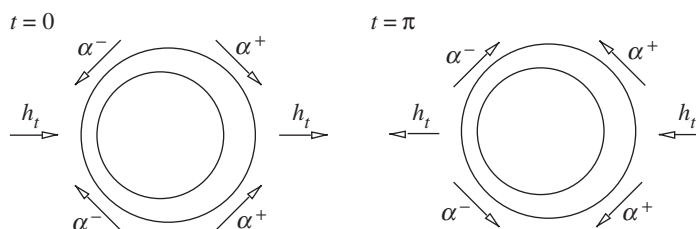


Figure 11. A second decay mechanism of the fundamental mode. The capillary pressure gradients from figure 10*b* act on the steady shape $\gamma \cos \theta$ to create rates of change of the fundamental mode of the disturbance.

by an amount calculated to be $27\alpha\gamma^3 \cos \theta$. This contributes the remaining $27\alpha\gamma^2$ towards the total decay rate of $81\alpha\gamma^2$ (see (3.13) with $\alpha \ll 1$). In dimensional terms, the fundamental mode in the disturbance decays over a time $\omega^2 \mu^3 a^6 / \rho^2 g^2 \sigma h_0^7$.

References

- Ashmore, J. J., Hosoi, A. E. & Stone, H. A. 2003 The effect of surface tension on rimming flows in a partially filled cylinder. *J. Fluid Mech.* **479**, 65–98.
- Hansen, E. B. & Kelmanson, M. A. 1994 Steady, viscous, free-surface flow on a rotating cylinder. *J. Fluid Mech.* **272**, 91–107.
- Heck, A. 1996 *Introduction to Maple*, 2nd edn. Springer.
- Kuiken, H. K. 1990 Viscous sintering: the surface-tension-driven flow of a liquid form under the influence of curvature gradients at its surface. *J. Fluid Mech.* **214**, 503–515.
- Moffatt, H. K. 1977 Behaviour of a viscous film on the outer surface of a rotating cylinder. *J. Mec.* **187**, 651–673.
- Peterson, R. C., Jimack, P. K. & Kelmanson, M. A. 2001 On the stability of viscous free-surface flow supported by a rotating cylinder. *Proc. R. Soc. Lond. A* **457**, 1427–1445.
- Pukhnachev, V. V. 1977 Motion of a liquid film on the surface of a rotating cylinder in a gravitational field. *Z. Prikl. Mekh. Tekh. Fiz.* **3**, 78–88. (Transl. 1977 *J. Appl. Mech. Tech. Phys.* **18**, 344–351.)
- Tirumkudulu, M. & Acrivos, A. 2001 Coating flows within a rotating horizontal cylinder: lubrication analysis, numerical computations, and experimental measurements. *Phys. Fluids* **13**, 14–19.
- Wilson, S. D. R. & Williams, J. 1997 The flow of a liquid film on the inside of a rotating cylinder, and some related problems. *Phys. Fluids* **9**, 2184–2190.

